Ruthenium(II) Complex-Photosensitized Multifunctionalized Porous Silicon Nanoparticles for Two-Photon Near-Infrared Light Responsive Imaging and Photodynamic Cancer Therapy

Nikola Ž. Knežević, Vanja Stojanovic, Arnaud Chaix, Elise Bouffard, Khaled El Cheikh, Alain Morère, Marie Maynadier, Gilles Lemercier, Marcel Garcia, Magali Gary-Bobo, et al.

Journal of Materials Chemistry B J. Mater. Chem. B, 2016, 4, 1337-1342

Article

Ruthenium(II) Complex-Photosensitized Multifunctionalized Porous Silicon Nanoparticles for Two-Photon Near-Infrared Light Responsive Imaging and Photodynamic Cancer Therapy

Received 00th January 20xx,
Accepted 00th January 20xx

DOI: 10.1039/x0xx00000x

www.rsc.org/

Nikola Ž. Knežević,[a] Vanja Stojanovic,[b] Arnaud Chaix,[a] Elise Bouffard,[b] Khaled El Cheikh,[b] Alain Morère,[b] Marie Maynadier,[c] Gilles Lemercier,*[d] Marcel Garcia,[b] Magali Gary-Bobo,*[b] Jean-Olivier Durand[a] and Frédérique Cunin*[a]

Multifunctionalized porous silicon nanoparticles (pSiNP) containing novel Ru(II) complex-photosensitizer, polyethylene glycol moiety, and mannose molecules as cancer targeting ligands, are constructed and showcased for application in near infrared (NIR) light-responsive photodynamic therapy (PDT) and imaging of cancer. Exposure to NIR light leads to two-photon excitation of the Ru(II)-complex which allows efficient simultaneous cancer-imaging and targeted PDT therapy with the functionalized biodegradable pSiNP nanocarriers.

Introduction

Photodynamic therapy (PDT) is rapidly advancing anticancer therapy which is nowadays increasingly applied in the clinical praxis alongside surgery, radiotherapy and chemotherapy.[1] This treatment option involves administration of chemical photosensitizers (PSs) and exposure of the diseased tissue to light irradiation with appropriate wavelength to induce formation of highly cytotoxic singlet oxygen ($^1O_2$) and reactive oxygen species (ROS), to induce cell death. In recent years research efforts have been dedicated to utilize nanomaterials for PDT of cancer,[2-6] which would be beneficial in terms of increasing efficacy and reducing side effects of the treatment,[7] with the possibilities for simultaneous targeted treatments and real time diagnostics.[8] Porous silicon nanoparticles (pSiNPs) are among the most promising types of nanocarriers for biomedical applications since the first publication by M. J. Sailor in 2009 on their application for *in vivo* treatment.[9] Composed of pure silicium, pSiNPs are distinguished by their spontaneous degradability in aqueous environment. In addition, pSiNP is characterized by high specific surface area, high capacity for drug loading and surface functionalization, high biocompatibility and low toxicity *in-vivo*.[10] Furthermore, pSiNP is intrinsically fluorescent material which can be applied for imaging and real time diagnostics even without the need for surface-functionalization.[10,11]

During the past decades, various types of PS molecules such as porphyrin,[2] phthalocyanine,[12] chlorine[13] derivatives have been applied for PDT, which typically function by exposure to UV or visible light. However, the low light-penetration depth (millimeters) and occurrence of tissue photo-damage limits the applicability of this spectral range for PDT, which can be circumvent by application of near-infrared irradiation (NIR)(750-1100 nm), and particularly two-photon excitation (2PE) which is just emerging for PDT applications and allows deeper penetration in biological tissues (2 cm) and lower scattering losses. Furthermore 2PE allows a three dimensional spatial resolution, with a spatio-temporal control which are essential features for a very precise treatment of cancer using PDT.[14] One of the pathways for NIR-responsive PDT has been demonstrated in the literature through laser excitation (at 980 nm) of up-converting nanoparticles which than emit higher energy light for excitation of PS.[15-17] However, this process is not highly efficient, particularly at 980 nm excitation due to substantial absorption of light by water at this wavelength. Furthermore up-converting NPs are not biodegradable and they lack the three dimensional accuracy which is characteristic for the 2PE process. Several ruthenium(II) complexes have been shown recently as promising photosensitizers, demonstrating their capabilities for absorption in the visible and ultra violet spectrum, which occurs by one-photon excitation (1PE) mechanism, as well as for NIR excitation due to the existence of long-lived triplet

[a] Institut Charles Gerhardt Montpellier, UMR5253 CNRS-ENSCM-UM2-UM1, Ecole Nationale Supérieure de Chimie Montpellier, 8 rue de l'Ecole Normale, 34296 Montpellier, France
[b] Institut des Biomolecules Max Mousseron, UMR 5247 CNRS-UM1-UM2, 15 Avenue Charles Flahault, BP 14491, 34093 Montpellier Cedex 05, France
[c] NanoMedSyn, 15 Avenue Charles Flahault, BP 14491, 34093 Montpellier Cedex 05, France
[d] Institut de Chimie Moléculaire de Reims, UMR CNRS 7312, BP 1039, 51687, Reims, France
Correspondances to: Dr. F. Cunin (E-mail: frédérique.cunin@enscm.fr), Dr. M. Gary-Bobo, (E-mail: magali.gary-bobo@univ-montp1.fr), Dr. G. Lemercier (E-mail: gilles.lemercier@univ-reims.fr),
Electronic Supplementary Information (ESI) available: experimental section; characterization by DLS, UV/VIS, nitrogen sorption; degradability study, UV/VIS spectra, quantification of Ru(II) and mannose, Ru(II) leakage test, imaging and PDT with the Ru(II) complex, cytotoxicity. See DOI: 10.1039/x0xx00000x

metal-to-ligand charge transfer state (^{3}MLCT), which can be excited by 2PE mechanism.[18] Therefore, coordination compounds of ruthenium(II) have been showcased recently as biocompatible, potent molecules for NIR-responsive cellular imaging,[19] and for 2PE-PDT.[20,21] However, these molecular PSs lack the cancer-targeting capabilities, which are achievable with more complex PS-nanoparticle conjugates due to enhanced permeability and retention (EPR) effect,[22] and surface functionalization strategies with ligands specific for cancer-overexpressed receptors.[23] Moreover, the attachment of PS to the nanomaterial would increase the uptake of PSs by cancer cells, as it is typical for drug nanocarriers.[24] Hence, the increased uptake of PSs by cancer cells is expected to increase the yields of $^1O_2$ and ROS production within cancer cells, leading to enhanced therapeutic efficacies of PS-nanoparticle conjugates over individual PS molecules. The covalent conjugation of Ru(II) complexes to nanocarriers in order to improve 2PE-PDT applications has not been investigated yet. Recent study demonstrated applicability of single-wall carbon nanotubes (SWCNT) for delivery of Ru(II) photosensitizer to cancer cells, which in fact increased 2PE-PDT efficacy of the photosensitizer when compared to the treatment with the molecular PS.[25] However, in this composite material the photosensitizer was physically adsorbed to the surface of SWCNT with the risk of leakage from the SWCNT matrix, while no investigation was conducted on efficacy of 2PE-PDT upon functionalization with PEG and cancer-targeting ligands. Furthermore, SWCNT nanocarrier is not biodegradable as in the case of pSiNP-based therapeutics.

In this study, we report a novel Ru(II) complex for NIR (2PE)-responsive PDT, along with the first pSiNP-based material containing Ru(II) complex-PS covalently attached to its surface for 2PE-PDT and 2PE-imaging application assessments. In addition, surface functionalization with polyethylene glycol (PEG) moieties was performed, essential for improving dispersibility and biocompatibility, along with attachment of mannose molecules, for enabling selective targeting of tumor tissues (Scheme 1).[26] The newly synthesized ruthenium(II) complex ion $[Ru(5\text{-Fluo-Phen})_2(5\text{-E-Phen})]^{2+}$, (5-Fluo-Phen) = 5-dihexylfluorene-1,10-phenanthroline and (5-E-Phen) = 5-ethynyl-1,10-phenanthroline, was covalently attached on pSiNP, along with PEG and Mannose, and we characterize their capabilities for two-photon imaging and *in vitro* 1PE-PDT and 2PE-PDT on breast cancer cells (MCF-7) upon exposure to blue light (430 nm) and short pulses (3 x 1,57 s) of near infrared (800 nm) irradiation.

Experimental section

Surface functionalization of pSiNP with $[Ru(5\text{-Fluo-Phen})_2(5\text{-E-Phen})]^{2+}$

A mixture of **$[Ru(5\text{-Fluo-Phen})_2(5\text{-E-Phen})](PF_6)_2$** (10 mg) in 10 ml of dry THF was prepared and suspension of pSiNP (70 mg) in dry THF (10 ml) was added. The reaction suspension was degassed for 30 min and refluxed at 50 ˚C under nitrogen atmosphere for 18 h. The product was then centrifuged at 14 000 rpm for 30 min, washed with THF three times, once with ethanol and kept suspended in ethanol until further use.

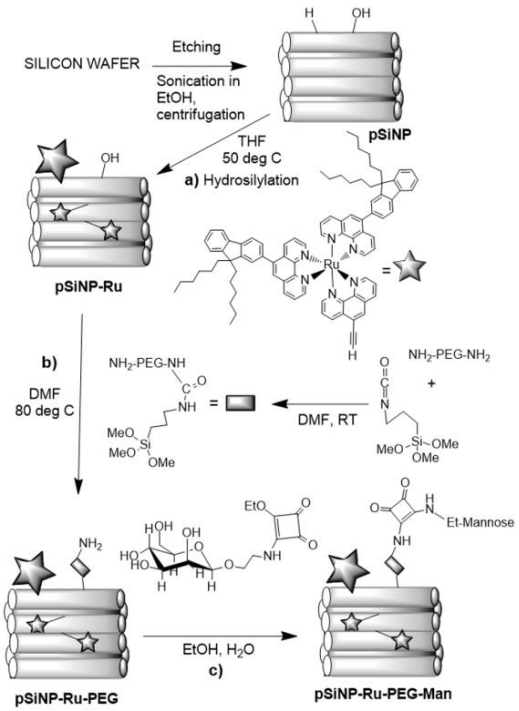

Scheme 1. Reaction pathways for the construction of the materials; a) hydrosilylation of $[Ru(5\text{-Fluo-Phen})_2(5\text{-E-Phen})]^{2+}$ to the surface through the terminal alkyne moiety, followed by b) silanization of surface hydroxyls with amine-terminated PEG and c) attachment of mannose through squarate moiety.

Attachment of ICPES-PEG to the surface of the pSiNP-Ru

The suspension of pSiNP-Ru (50 mg) in EtOH was centrifuged at 14 000 rpm for 30 minutes, washed once with dry DMF and redispersed in dry DMF (10 ml). A second flask containing O,O'-Bis(3-aminopropyl)polyethylene glycol (M~1.500, 0.15 g, 0.1 mmol) in 5 mL of dry DMF was prepared and isocyanopropyltriethoxysilane (ICPES) (26 μL, 0.1 mmol) was added dropwise under vigorous stirring. The reaction was stirred under nitrogen atmosphere for 3h and the suspension containing pSiNP-Ru was added. The reaction mixture wasdegassed for 30 min and refluxed at 80 ˚C for 18 h. The product (pSiNP-Ru-PEG) was centrifuged, washed three times with DMF and two times with ethanol. The material pSiNP-Ru-PEG was kept in the form of suspension in ethanol until further use.

Attachment of mannoseethylsquarate to pSiNP-Ru-PEG

Mannoseethylsquarate (17 mg, 49 μmol) was dissolved in 10 mL of demineralized water and added to the suspension ofpSiNP-Ru-PEG (47 mg) in ethanol (10 mL). The suspension was degassed for 30 min and refluxed at 80 ˚C for 18 h. The product was centrifuged at 14 000 rpm for 30 minutes, washed three times with EtOH, resuspended and kept in ethanol until further use.

Cell cultures

Human breast cancer cells MCF-7 (purchased from ATCC) were cultured in DMEM supplemented with 10% fetal bovine serum and 50 μg·mL^{-1} gentamycin. All cells were allowed to grow in humidified atmosphere at 37°C under 5% CO_2. For *in vitro* experiments, cells were seeded into a 384 multiwell glass bottomed plate (thickness 0.17 mm), with a black polystyrene frame. One day after seeding cells were treated at 80 μg·mL^{-1} concentration with 4 different nanostructures – porous silicon nanoparticles (pSiNP), porous silicon nanoparticles functionalized with ruthenium (pSiNP-Ru), porous silicon nanoparticles functionalized with ruthenium and polyethylene glycol (pSiNP-Ru-PEG) and porous silicon nanoparticles functionalized with ruthenium, PEG and mannose (SiNP-Ru-PEG-Man); and at 2.1 μg·mL^{-1} concentration with Ru(5-Fluo-Phen)$_2$(5-E-Phen)](PF$_6$)$_2$. Cells were incubated 5 h and then irradiated for 1 photon or 2 photon excitation (1PE or 2PE). 1PE was performed on LEICA DM IRB microscope at 420-440 nm wavelengths during 20 min. 2PE was performed on LSM 780 confocal microscope at 800 nm in the duration of 3 x 1,57 s. To measure the cell death, MTS assay was performed 48 h after irradiation and results were read on Thermo scientific multiscan FC instrument at the absorbance of 492 nm.

For two photon imaging cells were incubated 5 h with 80 μg/mL nanoparticles and 2.1 μg·mL^{-1} Ru(5-Fluo-Phen)$_2$(5-E-Phen)](PF$_6$)$_2$. Cell membranes were co-stained with Cell maskTM Orange plasma membrane stain in the concentration of 1 μl·mL^{-1} and after 15 min of incubation on 37˚C and 5% CO_2 cells were washed with Gibco DMEM (1x) and observed on LSM 780 Zeiss confocal microscopy (63x oil). Cell membranes were visualized in green at 560 nm, and NPs were visualized at 800 nm.

Results and Discussion

The pSiNP were constructed according to the published procedureby electrochemical etching of boron doped silicon wafer in an ethanolic hydrofluoric acid (HF) electrolyte, then electropolished in order to remove the porous silicon layer.[9] Afterwards, the obtained porous silicon was fractured by ultrasonication for 16 hours and microparticulate fragments were separated from the nanoparticles (pSiNP) by centrifugation.[11] The pSiNP were then characterized by Transmission Electron Microscopy (TEM), which reveals particles of diameter range 50-450 nm and their mesoporous texture (Figure 1a,b).

Absorption spectrum of pSiNP reveals broad band in the UV region which also extends into visible portion of the spectrum (Figure S1a). Nitrogen adsorption and desorption measurements showed that pSiNP has a mesoporous structure with high specific surface area of 560 m²/g and a BJH (Barrett-Joyner-Halenda) desorption average pore diameter of 12.3 nm (Figure S1.b). The dynamic light scattering (DLS) revealed the average size of the pSiNP at 226 nm with polydispersity of 0.30, measured by intensity percent of scattered light

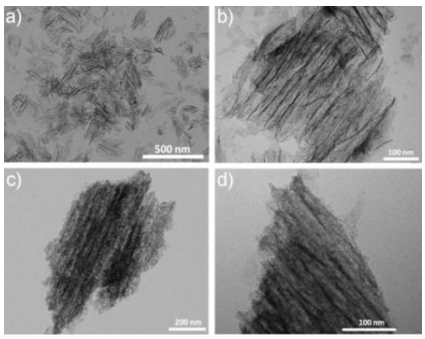

Figure 1. Transmission electron micrographs of pSiNP (a, b) and pSiNP-Ru-PEG-Man (c, d)

(Figure S1.c). However, the corresponding value revealing scattering normalized to the number of particles of specific diameter indicates that most of the particles have a diameter less than 100 nm, with the most prevalent at 79 nm (Figure S1.d).

Biodegradability of pSiNP was confirmed by stirring the material in aqueous suspension for a prolonged time and by measuring the mass of the centrifuged material (Figure S2). The result reveals that mass of the material decreases over the measured period of 10 days which indicates slow degradation of pSiNP by aqueous hydrolysis. We synthesized the novel photosensitizer ruthenium(II) coordination complex ion [Ru(5-Fluo-Phen)$_2$(5-E-Phen)]$^{2+}$ by ligand substitution in DMF solution and attached it to the surface of pSiNP by hydrosilylation of the terminal alkyne group of the 5-E-Phen ligand to the Si-H surface moieties on pSiNP, which yielded pSiNP-Ru material (Scheme 1). Attachment of bifunctionalized PEG moiety was than performed by coupling its one amine end to the isocyanatopropyltriethoxysilane (ICPES) and subsequent grafting on the surface of pSiNP-Ru through silanization to obtain pSiNP-Ru-PEG material. Finally, mannoseethylsquarate was covalently bonded to the other end of surface attached PEG moieties though nucleophilic substitution on the squarate moiety and yielded pSiNP-Ru-PEG-Man material. The attachment of all functional groups was confirmed by DRIFT and zeta potential measurements (Figure 2). After the hydrosilylation of the freshly etched pSiNP with the Ru(II) complex, new intense bands appeared at 2930 cm^{-1} and 2860 cm^{-1} which correspond to the stretching vibrations of C-H bonds. In addition, aromatic and aliphatic carbon-carbon stretching vibration bands are observed at 1450 cm^{-1} and 1380 cm^{-1}, respectively, arising from the attached Ru(II) complex. Concomitantly, intensity increase of the broad band centered at 1055 cm^{-1} which arises from the stretching Si-O vibrations, along with the appearance of broad band above 3000 cm^{-1}, corresponding to the stretching O-H vibrations, points to an occurrence of simultaneous competing oxidation reaction of the surface Si-H during the hydrosilylation reaction. In case of the pSiNP-Ru-PEG material a new band appearing at 1570 cm^{-1}, assignable to the amide moiety formed in the reaction between ICPES and NH_2-PEG-NH_2, indicates successful coupling

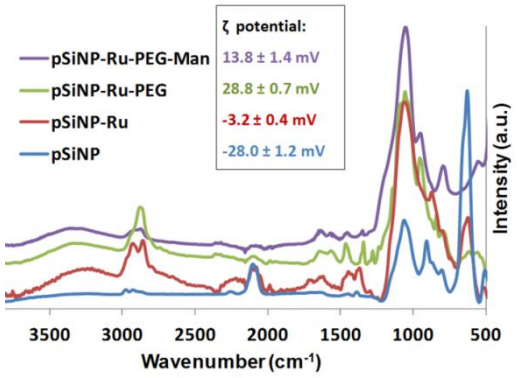

Figure 2. DRIFT spectra of the synthesized materials. Inset shows values for ζ potential of the corresponding materials

of pSiNP-Ru with PEG moiety. After attachment of mannoseethysquarate to the pSiNP-Ru-PEG material a shoulder at 1180 cm^{-1} appears in the DRIFT spectrum, which points to the existence of the carbohydrate C-O bonds in the pSiNP-Ru-PEG-Man material. Zeta potential measurements further evidence the successful surface functionalizations (Figure 2 inset). The bare pSiNP material exhibited highly negative surface charge (-28 mV), which is due to partial oxidation of the surface and deprotonation of the surface silanols. After grafting the positively charged Ru(II) complex ion onto the pSiNP surface the zeta potential value expectedly changes to less negative charge (-3.2 mV). Further functionalization with PEG moieties leads to highly positively charged surface (28.8 mV) which indicates successful attachment of the functional group containing charged amine ending groups. After the attachment of mannose to these amine groups the surface charge expectedly decreases to 13.8 mV. Transmission electron micrographs of the pSiNP-Ru-PEG-Man material (Figure 1c,d) reveal that the mesoporous texture of the material did not change after the functionalization reactions. Concentration of the Ru(II) complex was determined in all materials upon complete dissolution of the silicon carrier in 1M KOH:EtOH solution, by UV-Vis spectroscopy (Figure S3). Similarly, the mannose content in pSiNP-Ru-PEG-Man was determined after complete dissolution of the material in 1M KOH, followed by adjustment of previously published colorimetric method (Figure S5).[27] The measured values quantified in the form: quantity of the attached moiety/mass of the parent material, are as follows: Quantity of $[Ru(5\text{-}Fluo\text{-}Phen)_2(5\text{-}E\text{-}Phen)]^{2+}$ in: pSiNP-Ru: 18.0 $\mu g \cdot mg^{-1}$ (13.6 nmol/mg), pSiNP-Ru-PEG: 17.2 $\mu g \cdot mg^{-1}$ (13.0 nmol/mg), pSiNP-Ru-PEG-Man: 16.0 $\mu g \cdot mg^{-1}$ (12.0 nmol/mg), quantity of mannose ethyl squarate moiety in pSiNP-Ru-PEG-Man: 45.2 $\mu g \cdot mg^{-1}$ (147 nmol/mg). The mass *ratio* of Ru(II) in the materials expectedly decreases upon attachment of the additional functional groups which increase the total mass of the nanoparticles.

The efficacy of 1PE and 2PE photodynamic treatment with suspensions of pSiNP, pSiNP-Ru, pSiNP-Ru-PEG, and pSiNP-Ru-PEG-Man was investigated *in vitro* on breast cancer cell line MCF-7. All synthesized materials exhibited high dispersion stability in aqueous environment, with no evidence of precipitation. Cytotoxicity evaluation of the prepared materials without exposure to light is shown on Figure S7. In case of 1PE-PDT experiments the cells were treated at 80 $\mu g \cdot mL^{-1}$ with the series of nanomaterials and incubated for 5 h, after which the cells were exposed to blue light irradiation (420-440 nm, 14 $J \cdot cm^{-2}$) for 20 min. After two days of incubation, a cell proliferation assay (MTS) was performed to determine the phototoxicity of the different functionalized materials (Figure 3a). Upon monophotonic excitation with blue light (1PE-PDT) the non-functionalized pSiNP induced 13% of cell mortality. However, in the case of the 1PE-PDT with functionalized materials, more efficient cell mortality was noted, i.e. 43%, 26% and 21% for pSiNP-Ru, pSiNP-Ru-PEG and pSiNP-Ru-PEG-Man, respectively. These results show the ability of the pSiNP-based materials to generate $^1O_2$ and ROS under monophotonicexcitation. In addition, the photodynamic efficiency of the Ru(II) complex under 1PE can be evidently increased when attached to the pSiNP compared to the free Ru(II) complex efficiency (Figure S8.a). This underlines the role of the pSiNP in the vectorization of the Ru(II) complex photosensitizer to the cells. Decrease in PDT efficacy of the materials in the order: pSiNP-Ru > pSiNP-Ru-PEG > pSiNP-Ru-PEG-Man can be rationalized by the decreasing PS (Ru(II) complex) content in the same order.

In vitro 2PE-PDT experiments using the same pSiNP-based materials were also performed at the treatment concentration of 80 $\mu g \cdot mL^{-1}$ and pre-incubation for 5 h with MCF-7 cancer cells. Two-photon excitation was achieved using a Carl Zeiss confocal two-photon microscope (maximal laser input power 3 W). The wells were irradiated by 3 laser pulses of 1.57 s each at the irradiation wavelength of 800 nm, using the 10-fold magnification/objective 0.3 EC Plan-Neofluar. Two days after irradiation, the percentage of living cells was determined by MTS assay (Figure 3b). The results reveal that two-photon excitation is also a viable option to induce PDT in cancer cells.

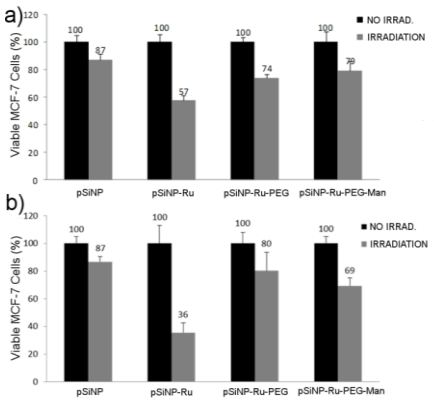

Figure 3. *In vitro* photodynamic effect of pSiNP, pSiNP-Ru, pSiNP-Ru-PEG and pSiNP-Ru-PEG-Man on MCF-7 cells. a) 1PE irradiation (420-440 nm, 14 $J \cdot cm^{-2}$, for 20 min); b) 2PE irradiation (800 nm, 3 scans of 1.57 s). Bar graphs represent means of triplicates ± standard deviation. Statistical analysis was performed using the Student's test to compare paired groups of data. *: $p < 0.05$ was considered to be statistically significant.

Viability of the cancer cells decreased by 13% in case of pSiNP-treated cells which indicates that this material can indeed induce formation of cytotoxic $^1O_2$ and ROS upon the two-photon excitation.[11] In comparison, in the case of the treatment with Ru(II)-photosensitizer-functionalized pSiNP, viability of the cancer cells decreased to 36 % which clearly shows the ability of the Ru(II) complex to increase the efficacy of pSiNP material for PDT upon near-infrared irradiation. In the case of 2PE the photodynamic effect of the pSiNP-Ru is significantly enhanced in comparison to the 2PE-PDT efficiency of the free Ru(II) complex (Figure S6.b), and to the efficiency ofbare pSiNP. Additional surface functionalization with PEG moieties unexpectedly decreases 2PE-PDT efficacy significantly. However, the presence of mannose is clearly beneficial as the viability of the cells treated with pSiNP-Ru-PEG-Man decreased to 69%, a significant difference to the viability of non-irradiated cells ($p < 0.05$), which is not the case for pSiNP-Ru-PEG-treated cells. This result can be ascribed to the better cell-internalization of the nanoparticles containing mannose moieties. Hence, we demonstrate in this study that even though the presence of PEG moiety hinders the photodynamic efficiency of the PS-functionalized pSiNP under 2PE, the presence of cancer-targeting mannose moiety is capable of overcoming this adversity through increased cell uptake. This result is promising en route for clinical application of nanomaterials for 2PE PDT, considering that PEG, or similar stealth-enabling molecules, are necessary constituents of nanotherapeutics for avoiding premature clearance from a biological environment.

In order to assess the capabilities of the prepared materials for two-photon imaging, the non-functionalized pSiNPs and functionalized-pSiNPs were incubated for 5 h at a concentration of 80 $\mu g \cdot mL^{-1}$ with breast cancer cells (MCF-7) and the two-photon fluorescence imaging of living MCF-7 cells was performed at 800 nm excitation wavelength with a Carl Zeiss two-photon confocal microscope (Figure 4). As evident, pSiNP material could not be detected by this method (Figure 4a) while the red color of Ru(II)-complex-containing materials was observed by the two-photon fluorescence imaging (Figure 4b-d, Figure S5.c for Ru(II) complex). Moreover, the two-photon imaging confirmed successful endocytosis of the PS-functionalized materials by MCF-7 cells and the uptake of pSiNP-Ru-PEG-Man was clearly more efficient than the uptake of pSiNP-Ru-PEG, which further supports the applicability of mannose as cancer-targeting moiety. The usefulness of PEG moiety is also evident by comparing the images of the cells treated with PEG-lacking pSiNP-Ru material and PEG-containing materials. Namely, PEG moiety contributed to better dispersion of the nanoparticles, which would be beneficial for prolonged blood circulation of the functionalized nanotherapeutics.

Conclusions

We have successfully constructed porous silicon-based nanomaterial functionalized with $[Ru(5\text{-Fluo-Phen})_2(5\text{-E-Phen})]^{2+}$ as a photosensitizer, polyethylene glycol moiety for improving the biocompatibility, and with mannose molecules as targeting moieties for photodynamic therapy of cancer. The multifunctionalized-pSiNPs exhibit potent capabilities for two-photon imaging of MCF-7 cells. Cytotoxic effects of the synthesized materials were demonstrated by exposing the treated cancer cells to blue and near infrared light irradiation, which led to 1PE- and 2PE-induced cancer cell death, respectively. The obtained results are promising for improvement of PDT therapy and further work is ongoing for optimization of pSiNP-based PDT nanotherapeutics for *in vivo* treatment of cancers.

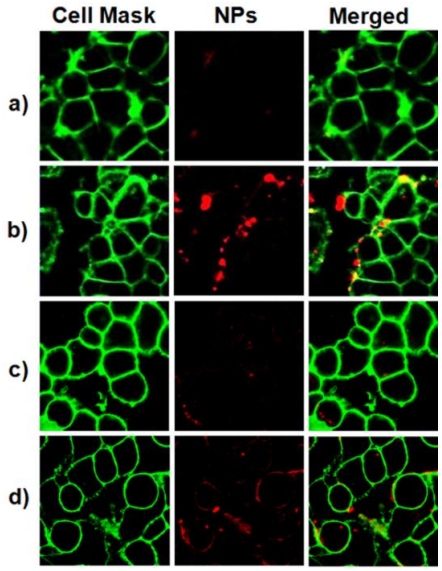

Figure 4. Multiphoton imaging of living MCF7 cells, incubated 5 h with 80 μg/mL nanoparticles (a) pSiNP, b) pSiNP-Ru, c) pSiNP-Ru-PEG, d) pSiNP-Ru-PEG-Man) and co-stained with a membrane marker (green). Fluorescence images were captured with spectral detector during a 800 nm two-photon excitation. Photos are representative of at least 3 independent experiments. Left: cell membrane staining, middle: nanomaterial, right: merge of the two images.

Acknowledgements

The ANR (Agence Nationale pour la Recherche, programme Blanc inter I SIMI 10, edition 2012) is gratefully acknowledged. The authors thank T. Cacciaguerra for the TEM imaging. N. Z. Knezevic and V. Stojanovic contributed equally to this work.

References

1 P. Agostinis, K. Berg, K. A. Cengel, T. H. Foster, A. W. Girotti, S. O. Gollnick, S. M. Hahn, M. R. Hamblin, A. Juzeniene, D. Kessel, M. Korbelik, J. Moan, P. Mroz, D. Nowis, J. Piette, B. C. Wilson and J. Golab, *Ca-Cancer J. Clin.*2011, **61**, 250.

2 E. Secret, M. Maynadier, A. Gallud, M. Gary-Bobo, A. Chaix, E. Belamie, P. Maillard, M. J. Sailor, M. Garcia, J.-O. Durand and F. Cunin, *Chem. Commun.* 2013, **49**, 4202.

3 P. Couleaud, V. Morosini, C. Frochot, S. Richeter, L. Raehm and J.-O. Durand, *Nanoscale* 2010, **2**, 1083.

4 W. Fan, B. Shen, W. Bu, F. Chen, Q. He, K. Zhao, S. Zhang, L. Zhou, W. Peng, Q. Xiao, D. Ni, J. Liu and J. Shi, *Biomaterials* 2014, **35**, 8992.
5 L. Sun, Y. Zang, M. Sun, H. Wang, X. Zhu, S. Xu, Q. Yang, Y. Li and Y. Shan, *J. Colloid Interface Sci.* 2010, **350**, 90.
6 M. Gary-Bobo, O. Hocine, D. Brevet, M. Maynadier, L. Raehm, S. Richeter, V. Charasson, B. Loock, A. Morere, P. Maillard, M. Garcia and J. O. Durand, *Int. J. Pharm.*2012, **423**, 509.
7 Z. Wang, X. Hong, S. Zong, C. Tang, Y. Cui and Q. Zheng, *Sci. Rep.* 2015, **5**, 12602.
8 J. Hu, Y. a. Tang, A. H. Elmenoufy, H. Xu, Z. Cheng, X. Yang, *Small* 2015, **11**, 5860.
9 J. H. Park, L. Gu, G. von Maltzahn, E. Ruoslahti, S. N. Bhatia and M. J. Sailor, *Nat. Mater.* 2009, **8**, 331.
10 E. J. Anglin, L. Cheng, W. R. Freeman and M. J. Sailor, *Adv. Drug Delivery Rev.* 2008, **60**, 1266.
11 E. Secret, M. Maynadier, A. Gallud, A. Chaix, E. Bouffard, M. Gary-Bobo, N. Marcotte, O. Mongin, K. El Cheikh, V. Hugues, M. Auffan, C. Frochot, A. Morère, P. Maillard, M. Blanchard-Desce, M. J. Sailor, M. Garcia, J.-O. Durand and F. Cunin, *Adv. Mater.* 2014, **26**, 7643.
12 S. Ogura, K. Tabata, K. Fukushima, T. Kamachi and I. Okura, *J. Porphyrins Phthalocyanines* 2006, **10**, 1116.
13 D. J. Lee, S. Y. Park, Y. T. Oh, N. M. Oh, K. T. Oh, Y. S. Youn and E. S. Lee, *Macromol. Res.* 2011, **19**, 848.
14 R. K. P. Benninger and D. W. Piston, Current protocols in cell biology / editorial board, Juan S. Bonifacino ... [et al.], 2013, **0 4**, Unit-4.1124.
15 X.-F. Qiao, J.-C. Zhou, J.-W. Xiao, Y.-F. Wang, L.-D. Sun and C.-H. Yan, *Nanoscale*, 2012, **4**, 4611.
16 L. Zeng, L. Luo, Y. Pan, S. Luo, G. Lu and A. Wu, *Nanoscale*, 2015, **7**, 8946.
17 X. Zhang, P. Yang, Y. Dai, P. a. Ma, X. Li, Z. Cheng, Z. Hou, X. Kang, C. Li and J. Lin, *Adv. Funct. Mater.*, 2013, **23**, 4067.
18 C. Girardot, G. Lemercier, J. C. Mulatier, J. Chauvin, P. L. Baldeck, C. Andraud, *Dalton Trans.* 2007, 3421; M. Four, D. Riehl, O. Mongin, M. Blanchard-Desce, L. M. Lawson-Daku, J. Moreau, J. Chauvin, J. A. Delaire and G. Lemercier, *Phys. Chem. Chem. Phys.* 2011, **13**, 17304.
19 14 W. C. Xu, J. R. Zuo, L. L. Wang, L. N. A. Ji, H. Chao, *Chem. Commun.* 2014, **50**, 2123.
20 H. Huang, B. Yu, P. Zhang, J. Huang, Y. Chen, G. Gasser, L. Ji and H. Chao, *Angew. Chem. Int. Ed.*, 2015, **54**, 14049.
21 S. C. Boca, M. Four, A. Bonne, B. van der Sanden, S. Astilean, P. L. Baldeck, G. Lemercier, *Chem. Commun.* 2009, 4590.
22 K. Greish, *Methods Mol. Biol.,* 2010, **624**, 25.
23 N. Ž. Knežević, J.-O. Durand, *ChemPlusChem*, 2015, **80**, 26.
24 H. C. Arora, M. P. Jensen, Y. Yuan, A. Wu, S. Vogt, T. Paunesku and G. E. Woloschak, *Cancer Res.* 2012, **72**, 769.
25 P. Zhang, H. Huang, J. Huang, H. Chen, J. Wang, K. Qiu, D. Zhao, L. Ji and H. Chao, *ACS Appl. Mater. Inter.* 2015, **7**, 23278.
26 M. Gary-Bobo, Y. Mir, C. Rouxel, D. Brevet, I. Basile, M. Maynadier, O. Vaillant, O. Mongin, M. Blanchard-Desce, A. Morère, M. Garcia, J.-O. Durand, L. Raehm, *Angew. Chem. Int. Ed.* 2011, **50**, 11425.
27 M. DuBois, K. A. Gilles, J. K. Hamilton, P. A. Rebers and F. Smith, *Anal. Chem.*1956, **28**, 350.

